Shandonay Kenzie (Orcid ID: 0000-0003-1994-5576)

MORPHOLOGY AND STRATIGRAPHY OF AEOLIAN SAND STRINGERS IN SOUTHEAST MINNESOTA AND WESTERN WISCONSIN, USA

*Kenzie L. Shandonay[1] (kshandon@asu.edu)
Mark W. Bowen[2] (mark.bowen@mnsu.edu)
Phillip H. Larson[2] (phillip.larson@mnsu.edu)
Garry L. Running[3] (runningl@uwec.edu)
Tammy Rittenour[4] (tammy.rittenour@usu.edu)
Richard Mataitis[2] (richardmataitis@gmail.com)

(1) School of Geographical Sciences and Urban Planning, Arizona State University, Tempe, AZ, 85282, (2) Department of Geography, Earth Science Programs, and EARTH Systems Laboratory, Minnesota State University, Mankato, Mankato, MN 56001, (3) Department of Geography and Anthropology, University of Wisconsin-Eau Claire, Eau Claire, WI 54701, (4) Department of Geosciences, Luminescence Laboratory, Utah State University, Logan, UT 84322

Ethics/integrity statement:

Authors declare no conflicts of interest or other ethical constraints related to conducting or publishing this research.

Acknowledgements and Funding:

We would like to thank Dr. Andrew Wickert and Dr. Randy Schaetzl for their helpful discussions and thoughts regarding this research and the regional importance of sand stringers. We would like to thank Dr. Carl

William Zanner, whose pioneering work on these landforms paved the way for this research. Special thanks to landowners for providing access to their properties.

This research was partially funded by a Minnesota State University, Mankato (MNSU) Graduate Student Research Grant, MNSU Department of Geography James F. Goff Research Award, MNSU Department of Geography George J. Miller Scholarship, MNSU Department of Geography Dr. Mary T. Dooley Field Studies Award, and a MNSU Faculty Research Grant.

Abstract

Sand stringers are subtle, aeolian landforms that reach 100's to 1000's of meters in length and lack a slipface. While 100's of sand stringers exist beyond the last glacial maximum margin in the upper Midwest, USA, little is known about the timing and nature of their formation. This research characterizes the morphology and stratigraphy and provides geochronological data from two sand stringers in the upper Mississippi River basin in Minnesota and Wisconsin.

The sand stringers investigated have similar west-northwest to east-southeast orientations and are located ~100 km from each other on uplands west and east of the Mississippi River valley. The sand stringer in Goodhue County, Minnesota (GC site), is ~870 m long and 50-80 m wide. To the east, the sand stringer in Eau Claire County, Wisconsin (ECC site), is ~925 m long and 30-50 m wide. The main body of GC sand stringer is characterized by a ~80-270-cm-thick silt-rich surface unit overlying a sandy unit that is underlain by a dark brown paleosol, while the main body of ECC sand stringer is sandier/coarser, stratified, and overlies outwash.

^{14}C ages, interpreted as minimums, at GC indicate formation began prior to 25-20 cal yr BP, while OSL and ^{14}C ages indicate ECC formed ~11.25–8.9 ka. We interpret the main body of GC as equivalent to Peoria Loess, with minor inputs of reworked outwash. We interpret ECC as composed of reworked outwash and local bedrock-derived sands. Pedogenesis at GC and ECC indicate stabilization with possible minor modification of near surface sediments through the Holocene. Differences in stratigraphy and chronology between the two sites highlight the complexity of aeolian systems in the upper Midwest, interpreted as indicative of the variety of sediment sources contributing to landform development via aeolian processes due to spatial and temporal variability in deglaciation and permafrost melting.

Keywords: soils, particle size, grain size distribution, radiocarbon,

optically stimulated luminescence, aeolian landforms

1. INTRODUCTION

Prior research has documented a variety of stabilized aeolian landforms (e.g., blowouts, climbing dunes, dune-dammed drainages, loess deposits, parabolic dunes, sand ramps, sand sheets, and sand stringers) throughout the landscapes of the upper Mississippi River basin (UMRB), USA (e.g., Hanson et al., 2015; Larson et al., 2008; Mason et al., 1999; Olson et al., 2008; Rawling et al., 2008; Schaetzl et al., 2018, 2014; Stanley and Schaetzl, 2011; Young, 2008; Zanner, 1999). Deposition of these aeolian sediments is suggested to have occurred during and following the Last Glacial Maximum (LGM) ~26.5-19 ka (Clark et al., 2009), and they represent part of a complex history of environmental change associated with regional deglaciation, periglacial conditions, and/or permafrost degradation (Mason, 2015; Mason et al., 1999; Rawling et al., 2008; Schaetzl et al., 2018, 2014; Stanley and Schaetzl, 2011; Zanner, 1999). Much of the prior literature on aeolian deposits in this region has focused on loess deposition, with relatively few studies focused on sand deposits and sandy aeolian landforms. Consequently, these aeolian deposits and landforms represent a relatively unexplored archive that could aid in our understanding of geomorphic and sedimentological response to climatic and environmental change post-LGM. In addition, understanding these LGM/post-LGM aeolian systems can provide insight into what might be expected in modern landscapes

experiencing deglaciation or permafrost degradation due to contemporary climate change.

Sand stringers, or sand streaks, are subtle, linear aeolian landforms that drape underlying topography and lack an identifiable slipface (McKee, 1979; Zanner, 1999). The terminology sand streak is commonly used to describe these forms identified by remote methodologies, while ground-based studies commonly use the term sand stringers. They have been identified in a variety of geographic locales like the Lagoa Dune Field, Brazil (Bigarella, 1979), northwest Sahara, Mauritania, the Navajo Reservation, northern Arizona, USA, and the northern Arabian Peninsula (Breed and Grow, 1979). These landforms are thought of as an elongate variety of sand sheet (McKee, 1979) and prior studies suggest they form in regimes of predominantly unimodal and strong winds (Breed and Grow, 1979), but little research has been done to determine the processes by which they form.

These poorly understood sandy aeolian landforms are also widely distributed throughout the UMRB, USA, beyond the LGM ice margin. They were identified as potential "linear dunes" in western Wisconsin via remote mapping by Schaetzl et al. (2018) and have also been identified in South Dakota, Minnesota, Iowa, and Illinois, USA (Follmer, 1978; Koch and Walters, 2004; Mason, 1992; Millet et al., 2018; Zanner, 1999). Due to prior research conducted in the UMRB on aeolian deposits, we use the term sand stringer for consistency in describing these landforms in this

study. A comprehensive analysis of sand stringers utilizing modern geospatial datasets has not been completed in the UMRB, leaving the number, orientation, and spatial distribution of sand stringers across this region uncertain. Preliminary work by Millett et al. (2018) and Mataitis (2020) suggested several hundred of these landforms exist.

Zanner (1999) is the only study to comprehensively investigate the distribution, morphology, sedimentary characteristics, stratigraphy, and depositional chronology of sand stringers. Zanner (1999) identified sand stringers in Minnesota, Iowa, and Illinois, but focused his investigation on Canfield Creek sand stringer (CC) in Fillmore County, Minnesota (Fig. 1). CC is ~2.3 km in length and oriented northwest-southeast. Fourteen stratigraphic units were identified within and below CC, and thermoluminescence (TL) ages of ca. 14.7-11.2 ka were obtained from depths of 81-150 cm within the main body of CC. Zanner (1999) hypothesized that the complex stratigraphy represented shifts in regional environmental conditions associated with ice margin fluctuations during the LGM and afterward.

The limited scope of Zanner's (1999) investigation to only one sand stringer in a region where they are widely distributed, and the use of TL dating (a geochronology method with high uncertainty; e.g. Noller et al., 2000) highlights the need for further investigation of these landforms in the UMRB. This is especially important given their potential significance as a record of paleoenvironmental and geomorphic change post-LGM

(Schaetzl et al., 2018; Zanner, 1999). The purpose of this research is to build on Zanner's (1999) work at CC by characterizing sand stringer morphology and investigating the internal stratigraphy, sedimentology, and depositional chronology within two representative sand stringers in the UMRB. Our objectives include: (1) calculating the morphometry (i.e., size and shape) using geographic information systems (GIS) and geospatial analysis techniques, (2) describing subsurface stratigraphy by collecting soil-sediment cores and completing detailed soil profile/core descriptions, (3) characterizing particle-size distribution for stratigraphic units using laser diffractometry techniques, and (4) utilizing numerical age data acquired from stratigraphic units via radiocarbon (^{14}C) and optically stimulated luminescence (OSL) dating to constrain the depositional chronology of these landforms.

2. METHODS

2.1 Regional Setting

Two linear landforms interpreted as aeolian sand stringers, one located in Goodhue County, Minnesota (GC) (44.460820° N, 92.703660° W) and the other in Eau Claire County, Wisconsin (ECC) (44.798570° N, 91.595660° W) (Fig. 1), were selected for this study given their accessibility, clear surface expression, and spatially distant geographic position relative to each other and CC investigated by Zanner (1999). Stringers were initially identified remotely by their distinct light tones on

color aerial imagery collected for the National Aerial Imagery Program and isolated, elongate form visible on LiDAR-derived hillshade digital elevation models. Roadside surveys and augering were conducted to confirm sites had morphology and stratigraphy consistent with sand stringers previously studied in the UMRB (e.g. Mason, 1992; Zanner, 1999).

GC is located within an agricultural field in a broad valley ~18 km southwest of Redwing, Minnesota, ~10 km south of the Cannon River, and ~18 km southwest of the Mississippi River (Figs. 1 and 2). ECC is located within an agricultural field on a broad upland ~8 km west of Eau Claire, Wisconsin, ~3 km north of the Chippewa River, and ~60 km northeast of the Mississippi River (Figs. 1 and 3). GC is ~65 km east of the former ice margins of the Des Moines Lobe (Lusardi et al., 2011) and ECC is ~50 km southwest of the Chippewa Lobe terminal moraine of the Laurentide ice sheet (Fig. 1) (Dalton et al., 2020). The locations of GC, ECC, and CC were not covered in glacial ice during the LGM but were likely influenced by permafrost conditions, possibly until ~14-12 ka (Clayton et al., 2001; Loope, 2012; Mason, 2015; Schaetzl et al., 2021; Zanner, 1999).

Soil-sediment cores collected from GC stringer and the surrounding valley confirm that sand deposits are thicker in the stringer than on the valley floor (Fig. 4), supporting our interpretation that GC is an aeolian sand stringer. At ECC, cores did not extend through the aeolian sand at any core location, so we cannot confirm that the stringer body is

composed of thicker accumulations of aeolian sand than the surrounding valley. However, given the distinct topographic expression, clearly visible light tones on several years of aerial imagery, and the entire feature is mapped as Kevilar sandy loam or Prissel loamy sand, it is likely that ECC is an aeolian sand stringer.

2.2 Sand Stringer Morphology

Sand stringers were mapped in a GIS by digitizing landform boundaries and creating polygons for each landform using LiDAR-derived hillshade digital elevation models. LiDAR data for Goodhue and Eau Claire counties were acquired from the USDA NRCS Geospatial Data Gateway (https://datagateway.nrcs.usda.gov/).

2.3 Sand Stringer Stratigraphy and Particle Size Distributions

A Giddings hydraulic coring machine was used to collect six soil-sediment cores at GC and seven soil-sediment cores at ECC (Table 1; Figs. 2 and 3). Cores were collected from a variety of landscape positions at both sites, including along the crests and shoulders of the sand stringers and the valley floor adjacent to each stringer. Cores were collected until refusal in 2.5-cm-diameter, clear, plastic liners, and capped, sealed, and transported to the EARTH Systems Laboratory at

Minnesota State University, Mankato for analysis. Core depth ranges from 145 cm to 313 cm at GC and from 177 cm to 289 cm at ECC (Table 1).

All cores were described following standard USDA National Soil Survey Center guidelines (Schoeneberger et al., 2012). Soil descriptions include horizonation, Munsell color, structure, visible roots, visible rocks, boundary distinctness, consistence, hand texture, and redoximorphic features. Samples were collected in 1-4 cm intervals, adjusting for stratigraphic complexity, for particle size analysis.

Particle-size distribution was analyzed via laser diffraction techniques using a Malvern Mastersizer 3000. The Malvern outputs results in a range of 0.01-2000 μm by relative percent per size class. Each sample was dried, gently disaggregated using a mortar and pestle, and passed through a 2 mm sieve before analysis via wet dispersion with sonication to disperse aggregates. Given the low organic matter and clay contents of samples, experiments showed that pre-treatment with hydrogen peroxide (H_2O_2) and sodium hexametaphosphate ($Na_6(PO_3)_6$) were not necessary. Textural class of each sample was determined using Triangle, a program that generates the correlative soil texture based on percent sand, silt, and clay using the USDA classification scheme (Gerakis and Baer, 1999).

2.4 Chronology of Sand Stringer Deposition

2.4.1. Optically Stimulated Luminescence Dating

Age control for ECC was established via optically stimulated luminescence (OSL) dating; due to logistical constraints associated with the COVID-19 pandemic and access restrictions from the landowner, it was not possible to collect OSL samples from GC. Samples for OSL dating were collected at ECC immediately adjacent to cores 1 and 6 (Fig. 3) at depths ranging from 145-275 cm. Exploratory augering was done next to each OSL sample location to determine optimal sediment to collect and to avoid potential for bioturbation. Samples were extracted at desired depths using a closed auger bit with an 8” aluminum conduit tube placed inside, which was capped and sealed upon removal. Dose rate and water content samples were collected from above and below each OSL sample.

Samples were submitted to the Utah State Luminescence Laboratory and were processed under dim amber safelight conditions. Sample processing for OSL dating of 150-250 μm fine quartz sand followed standard procedures involving sieving, hydrochloric acid (HCl) and bleach treatments to remove carbonates and organic material, heavy mineral separation at 2.72 g/cm^3, and acid treatments with hydrogen fluoride (HF) to isolate the quartz component. The purity of quartz samples was checked by monitoring response to infra-red stimulation to detect the presence of feldspar.

OSL samples were analyzed following the single-aliquot regenerative-dose (SAR) technique (Murray and Wintle, 2000) on small-aliquot (1 mm diameter, ~20-40 grains per disk) fine quartz sand. Luminescence measurements were performed on Risø TL/OSL Model DA-20 readers, with stimulation by blue-green light emitting diodes (LED) (470±30 nm) and the luminescence signal was detected through 7.5-mm UV filters (U-340) over 40 seconds (250 channels) at 125ºC with LED diodes at 90% power (36-45 mW/cm^2). Luminescence signals were calculated by subtracting the average of the last 5 seconds (background signal) from the sum of first 0.7 seconds (4 channels) of signal.

The equivalent dose (D_E) of radiation the sample received following deposition, or burial dose, was calculated from 27-32 aliquots per sample. Data from aliquots were rejected in age calculation if they had evidence of feldspar contamination, corrected signals from repeated doses >15% of unity or recuperation of the zero-dose point >10% of the natural signal. D_E distributions for each sample were largely symmetrical and had overdispersion (scatter beyond instrumental error) that range from 16% to 22% (Supplementary Figure 1). Representative D_E values for age determination were calculated using the Central Age Model (CAM) of Galbraith and Roberts (2012). The OSL age is reported at 2σ standard error and is calculated by dividing the D_E (in Grays, Gy) by the environmental dose rate (Gy/yra) that the sample has been exposed to

during burial. OSL ages are discussed in ka, or thousands of years before present, in this study.

Dose-rate calculations were determined by chemical analysis of the U, Th, K and Rb content using ICP-MS and ICP-AES techniques and conversion factors from Guérin et al. (2011). The contribution of cosmic radiation to the dose rate was calculated using sample depth, elevation, and latitude/longitude following Prescott and Hutton (1994). Dose rates are calculated based on water content, sediment chemistry, and cosmic contribution (Aitken and Xie, 1990; Aitken, 1998).

2.4.2 Radiocarbon Dating

We utilized AMS ^{14}C dating to establish age control for GC since OSL dating was not possible and to complement OSL dating at ECC. ECC exhibits clear evidence of translocation of organic matter throughout profiles, GC likely experienced translocation during formation, and deep roots could have contributed younger carbon at depth. Thus, all radiocarbon ages in this study are interpreted as minimum age for sediment deposition.

Five bulk-sediment samples from GC and four from ECC were collected from C horizons in cores, dried, ground, and all visible roots and other debris were removed. Samples were submitted to the National Ocean Sciences Accelerator Mass Spectrometry Lab (NOSAMS) for analysis. At NOSAMS, samples were treated to remove inorganic carbon

and mobile organic acid phases and combusted at high temperature to produce CO_2 and converted to graphite for analysis by accelerator mass spectrometry. Sample ages were corrected for fractionation compared to standards and reported following conventions described by Stuiver and Polach (1977) and Stuiver (1980).

Radiocarbon ages were calibrated to calendar ages using the online CALIB 8.2 Radiocarbon Calibration Program (Stuiver et al., 2021) (Table 2). Ages are reported as mean age plus/minus two standard deviations in calendar years before present (cal yr BP) or cal kyr BP (thousands of calendar years BP) for the highest probability distribution under the calibration curve.

3. Results

3.1 Sand Stringer Morphology

GC and ECC morphologies and orientations are generally similar to each other. GC is ~870 m long and 50-80 m wide, and ECC is ~925 m long and 30-50 m wide. GC has slightly greater relief than ECC, with a total relief of ~3-5 m from crest to valley floor along most of the crest; there is a pronounced peak ~10 m higher than the valley floor ~50 m from the northwest edge of the stringer and a pronounced swale ~1 m higher than the valley floor ~300 m from the northwest edge (Fig. 2). ECC has a total relief of ~1-4 m from crest to valley floor, and the crest is gently undulating and slopes with the valley floor to the northwest (Fig.

3). Bearings for GC and ECC are 117° and 112°, respectively, indicating the long axis of both sand stringers trends east-southeast.

3.2 Stratigraphy and Depositional Chronology

3.2.1 GC Sand Stringer

Soil coring at GC captured three stratigraphic units as indicated by distinct shifts in particle size, color, and/or structure, and particle size data reveal that it is primarily composed of silt with secondary inputs of sand (Fig. 4 and Supplementary Tables 1-6). Unit 1 consists of the Ap, A, B, BC, C, and C2 soil horizons and is predominantly classified as silt loam or sandy loam. Median grain size (D_{50}) ranges from 20-50 μm (i.e., coarse silt) for most of the samples within unit 1 (Supplementary Figure 2). The A horizon is 20-36 cm thick, dark brown with granular or weak subangular blocky structure, silt loam texture, and the upper ~15 cm has been disturbed by plowing. The B horizon is 18-29 cm thick with brown to dark yellowish-brown color, subangular to angular blocky structure, and silt loam to sandy loam texture. Cores 1, 2, and 5 have a ~20-30-cm thick silt loam to sandy loam BC horizon. The C and C2 horizons are ~100-200 cm thick, yellowish brown to dark yellowish brown, with weak subangular blocky structure or is structureless, and has predominantly silt loam and to a lesser extent sandy loam texture. At core 1, the C horizon is composed of 4-10-cm-thick alternating sandy loam and silt loam layers. Three of the six GC cores have increased sand content in the middle to

upper portion of unit 1: core 1 from ~50-130 cm (BC and C horizons), core 3 from ~25-125 cm (B and C horizons), and core 4 from ~25-90 cm (B and C horizons) (Fig. 4). Unit 1 is thickest at cores 1, 2, and 3, thinner at cores 4 and 5, and thinnest on the valley floor at core 6. Sediment samples taken from the base of unit 1 returned ^{14}C ages of 25,290 ± 670 cal yrs BP at a depth of 216 cm in core 3 and 22,470 ± 290 cal yrs BP at 188 cm in core 2 (Table 2). GC core 3 also returned an age of 9,090 ± 60 cal yrs BP at a depth of 118 cm.

Unit 2 consists of the 2C horizon and is composed of structureless sandy loam, loamy sand, and sand with rocks and pebbles throughout, iron staining and Fe-Mn nodules common, and brown to yellow brown color. Median grain size of unit 2 ranges from ~25 μm to ~275 μm (i.e., coarse silt to medium sand) (Supplementary Figure 2). At core 3, near the swale, the middle 50 cm of this unit is carbonate cemented (2Ck horizon); carbonates were not observed in any other cores. Unit 2 is greater than 1 m thick at cores 3 and 5; less than ~50 cm was retrieved at cores 1, 2, 4, and 6. Actual thickness of unit 2 is unknown due to inability to penetrate deeper during coring. On the stringer, only core 2 extended below unit 2 and captured the upper 25 cm of unit 3 (3C horizon), a very firm sandy loam with strong brown color, which was also captured in core 6 from the valley floor (Fig. 4). Median grain size of unit 3 ranges from 80-160 μm (i.e., very fine and fine sand) in core 2 and 40-130 μm (i.e., coarse silt to fine sand) in core 6 (Supplementary Figure 2).

Samples collected near the top of unit 3 returned radiocarbon ages of 21,660 ± 590 cal yrs BP at 122 cm in core 6 and 20,130 ± 350 cal yrs BP at 235 cm in core 2 (Table 2). The returned age at 235 cm is ~2,300 years younger than the returned age at 188 cm in core 2, which could be due to potential inputs of younger carbon.

Grain-size distributions of samples from the A, B, and C horizons within unit 1 at GC are bimodal (Supplementary Figure 3a). The primary peak is centered around ~20-50 μm (silt), and the secondary peak is centered around ~200-300 μm (i.e., fine to medium sand). Grain size distribution of unit 2 is also bimodal though coarser (Supplementary Figures 3b and 3c). For cores 1, 2, and 5, the primary peak is centered around ~200-300 μm with a distinct secondary peak centered around ~20-50 μm (Supplementary Figure 3b). Cores 3, 4, and 6 also have a primary peak centered around 200-300 μm but have a broad increase from ~2-80 μm (Supplementary Figure 3c).

3.2.2 ECC Sand Stringer

Soil cores at ECC also consist of three stratigraphic units as indicated by distinct shifts in particle size, color, and/or structure (Fig. 5, Supplementary Tables 7-13). Unit 1 is composed of ~60-100 cm of primarily sandy loam and silt loam with Ap-A-B/Bt-BC horizonation. The A horizon is 13-24 cm thick, dark brown to grayish brown, with granular or weak subangular blocky structure, and the upper ~15 cm has been

disturbed by plowing. The B horizon is 16-42 cm thick, brown to dark gray brown, with subangular blocky structure. All cores have a brown to dark yellowish brown BC horizon that is structureless or has weak subangular blocky structure and ranges in thickness from 12-52 cm. In cores 2, 3, and 6 unit 1 is dominated by sand, while silt dominates the middle portion of the unit (B, Bt, and BC horizons) in cores 1, 4, and 5 (Fig. 5). In core 7, on the valley floor adjacent to the stringer, silt dominates the upper portion of unit 1 (Ap, AB, and Bt horizons) and sand dominates the lower portion (BC horizon) (Fig. 5). Median grain size of the upper portion of unit 1 (Ap, A, B, and Bt horizons) ranges primarily from ~30-80 μm (i.e., coarse silt to very fine sand), while median grain size of the lower portion of unit 1 (BC horizons) ranges primarily from ~60-250 μm (i.e., very fine sand to fine sand) (Supplementary Figure 4). On the valley floor, the upper ~45 cm of unit 1 has a finer texture than the other cores, with a median particle size of 20-30 μm (i.e., coarse silt), while the lower portion of the unit is similar to other cores (Supplementary Figure 4). A sample collected from unit 1 in core 1 at a depth of 61 cm (~28 cm above the boundary with unit 2) returned a radiocarbon age of 1,310 ± 10 cal yrs BP (Fig. 5 and Table 2).

Underlying unit 1, is at least 86 cm of stratified sands; actual thickness of stratified sands is unknown due to inability to penetrate deeper during coring. All ECC cores contain a 60 cm to at least 110 cm thick stratified 2C horizon (unit 2) with loamy sand to sand texture and

intercalated 1-8-cm-thick iron oxide-enriched bands (i.e., pedogenic lamellae) with increased silt and clay content (Fig. 5). These pedogenic lamellae are dark brown with friable to firm consistence and have abrupt boundaries with interlayered structureless, loose, light brown or yellowish-brown sand. Pedogenic lamellae are common at the boundary between units 1 and 2. Percentages of sand for unit 2 are variable, ranging from ~15-97% and oscillating by more than 20% within a few centimeters (Fig. 5), and D50 ranges from ~50 μm (i.e., very fine sand) to 475 μm (i.e., medium sand) (Supplementary Figure 4). Core 4 differs slightly, with a lower sand content of 30-70% (Fig. 5) and D50 ranging from ~30 μm (i.e., coarse silt) to 300 μm (i.e., medium sand) (Supplementary Figure 4), and only three samples with D50 >100 μm.

Samples from unit 2 in core 1 returned ^{14}C ages of 6,290 ± 20 cal yrs BP at a depth of 94 cm and 7,990 ± 50 cal yrs BP at a depth of 128 cm. A sample collected at 91 cm in core 6 returned an age of only 1,990 ± 60 cal yrs BP, ~4,300 years younger than the sample from an equivalent depth in core 1. Three OSL samples were collected adjacent to core 1 and returned ages of 11.17 ± 1.64 ka at a depth of 153 cm, 10.14 ± 1.30 ka at 242 cm, and 11.25 ± 1.71 ka at 275 cm (Tables 3 and 4). The uppermost OSL sample was obtained from unit 2; the two lowermost samples were obtained from depths beyond what was retrieved from the Giddings-collected soil cores, but sediment descriptions indicate samples were collected from sediments consistent with unit 2. A single OSL sample

was collected from unit 2 adjacent to core 6 and returned an age of 8.86 ± 1.40 ka at a depth of 145 cm (Tables 3 and 4).

Within cores 3, 4, 5, and 6 a second stratified sand unit (3C horizon; unit 3) at least 50 cm thick was observed, with evidence of gleying in cores 3, 4, and 6. Unit 3 is similar to unit 2, with intercalated pedogenic lamellae, but unit 3 is composed of coarser sands and is denoted by a sharp increase in D50 (Supplementary Figure 4). The shift occurs in core 3 at 194 cm, core 4 at 130 cm, core 5 at 140 cm, and core 6 at 218 cm (Supplementary Figure 4). Cores 4, 5, and 6 also have gravels and pebbles present in the lower portion of unit 3.

Grain-size distributions for ECC are variable among cores but generally have multiple peaks ranging from ~10-1000 μm (silt to coarse sand) (Supplementary Figures 5 and 6). Unit 1 exhibits one of three distributions: (1) primary peak ~20-30 μm (silt) and secondary peak ~200-400 μm (fine to medium sand) (Supplementary Figure 5a), (2) primary peak ~100-400 μm (fine to medium sand) and secondary peak ~20-30 μm (silt) (Supplementary Figure 5b), or (3) wide distribution with approximately equal peaks ~20-30 μm (silt), ~100-200 μm (fine sand), and ~300-500 μm (medium sand) (Supplementary Figure 5c). Grain-size distributions for unit 2 are generally shifted to the coarser end than unit 1. Peaks range between ~100-500 μm (fine to medium sand), with tails skewed towards the fine end (Supplementary Figure 6a). Unit 3 is coarser than units 1 and 2, and samples typically have a unimodal peak ~300-

700 μm (medium to coarse sand) and only minor inputs below ~50 μm (silt and clay) (Supplementary Figure 6b). Throughout both stratified units, pedogenic lamellae exhibit similar grain size distributions as other layers.

4. DISCUSSION

4.1 Sand Stringer Morphology

At ~870-925 m in length, 30-80 m wide, and primarily 1-5 m of relief, GC and ECC have morphologies similar to other sand stringers described in the regional literature (Koch and Walters, 2004; Mason et al., 1999; Millet et al., 2018; Schaetzl et al., 2018; Zanner, 1999). Sand stringers have been described as: (1) 3-5 m in height, 20-100 m wide, and up to 20 km in length (Koch and Walters, 2004), (2) 1.5-3 m in height, ~100 m wide, and exceeding 1 km in length (Schaetzl et al., 2018), (3) 1.5-3 m in height, up to 100 m wide, and 10-100s of m in length (Millet et al., 2018), (4) 1-3 m in height, up to 50 m wide, and up to 7 km in length (Zanner, 1999), and (5) 1-3 m in height and several kilometers in length (Mason et al., 1999).

Previous studies note sand stringers in the region are predominantly oriented northwest-southeast (Koch and Walters, 2004; Mason et al., 1999; Millet et al., 2018; Schaetzl et al., 2018; Zanner, 1999). The sand stringers investigated in this study also have a northwest-southeast orientation. Some Midwestern aeolian studies note easterly wind flow off

the Laurentide Ice Sheet (COHMAP Members, 1988; Krist and Schaetzl, 2001; Vader et al., 2012), but these sites were directly adjacent to a west-east oriented portion of the Laurentide ice margin north and east of the UMRB. Based upon orientation of GC, ECC, CC, other sand stringers (Mataitis, 2020; Millet et al., 2018; Zanner, 1999), and a variety of aeolian landforms within western Wisconsin and southeastern Minnesota, the prevailing wind at the time of sand stringer formation was west-northwest (Mason et al., 1999; Millett, 2019; Rawling et al., 2008; Schaetzl et al., 2018; Stanley and Schaetzl, 2011; Zanner, 1999).

4.2 Stratigraphy and Depositional Chronology

4.2.1 GC Sand Stringer

We interpret median particle-size and the character of the grain-size distributions (Supplementary Figures 2 and 3) at GC to indicate unit 1 as the main body of the sand stringer and the predominantly siltier sediments consisting of reworked Peoria Loess. Peoria Loess is the predominant surficial deposit throughout much of Goodhue County, including ~2.5-10 m-thick-loess covering 67% to 100% of the land surface surrounding and immediately upwind of the sand stringer (Thorp and Smith, 1952). Additionally, several soil series formed in loess, including Mt. Carroll, Port Bryon, Seaton, and Timula soil series, are mapped surrounding and upwind of the stringer (Soil Survey Staff, 2011). Peoria Loess was deposited regionally 25-12 ka (Leigh and Knox, 1994),

and generally decreases in grain size from west to east across southeast Minnesota (Mason et al., 1994). Potential sources for Peoria Loess at the GC site include sediments from the pre-Wisconsinan Iowan erosion surface or Wisconsinan glacial outwash plains (Mason et al., 1994) derived from Des Moines Lobe meltwater. Outwash plains are likely sources as the Des Moines Lobe advanced to within ~65 km west of GC, and the Cannon River valley, a former meltwater drainage of the Des Moines Lobe (Hobbs and Setterholm, 1998), is ~10 km northwest of GC. Conversely, the Iowan erosion surface is primarily southwest of GC, and given the morphology, orientation, and prior regional aeolian literature, it is likely that west-northwesterly winds deposited these aeolian sediments.

Cores 1, 2, 3, and 4 from GC have increased sand content within the middle to upper portion of unit 1 (Fig. 4). The apparent upward coarsening of sediment size in the main body of GC is interpreted as sand that was deflated from surrounding glaciofluvial outwash or proximal sandy alluvial deposits (Hobbs and Setterholm, 1998). A sample near the middle of unit 1 returned a ^{14}C age from the Early Holocene (~9.1 cal kyr BP), while ^{14}C ages from the base of this unit are Late Pleistocene in age (~25.3-22.5 cal kyr BP; Table 2). Although these are best interpreted as minimum ages, it does suggest deposition and stringer formation began during the LGM, but we cannot determine when aeolian deposition ceased at GC.

Grain-size distributions for unit 2 indicate it is primarily composed of fine to medium sand with secondary inputs of silt (Supplementary Figures 3b and 3c). Unit 2 is interpreted as water-transported and reworked glacial outwash or local alluvial deposits based upon its coarser grain size (Figs. 4 and Supplementary Figure 2) and the inclusion of gravels (Supplementary Tables 1-6), while contemporaneous deposition of loess occurred in this stratigraphic unit. This loess may indicate the beginning of aeolian deposition in this landscape and the start of stringer formation. The valley floor GC is situated upon is mapped as pre-Wisconsin glaciation glaciofluvial and till deposits, and sandy alluvial deposits are mapped within 1 km of GC (Hobbs and Setterholm, 1998), providing a potential local source for coarser sediments in unit 2.

Cores 2 and 3 at GC captured the top of a brown to strong brown, sandy loam unit (unit 3), which we interpret as a paleosol that existed prior to sand stringer formation. Surficial geology indicates the paleosol formed on the Pierce Formation, an Illinois to Pre-Illinois glacial episode till underlying the area near GC (Hobbs and Setterholm, 1998). Given evidence of pedogenic modification (Supplementary Tables 2 and 6), we interpret unit 3 to represent a relatively stable surface prior to deposition of GC. Sediment samples collected from the top of unit 3 returned radiocarbon ages from the Late Pleistocene (Table 2). Although out of chronostratigraphic order with radiocarbon ages from the basal portions of unit 1 (~25.3-22.5 cal kyr BP), we interpret these ages, in conjunction

with the basal radiocarbon dates in unit 1, to suggest a possible time frame for initiation of aeolian deposition at GC between 25.3 and 20.1 cal kyr BP.

4.2.2 ECC Sand Stringer

ECC has greater sand content and coarser grain size distributions than GC (Fig. 5 and Supplementary Figure 4). Unit 2 is interpreted as the main body of ECC. Given the predominance of silt and fine sand in unit 1, medium to coarse sand in unit 2, and coarse sand with fine gravel and pebbles in unit 3, the units are interpreted as sourced from local bedrock and glacial outwash deposits (unit 3), reworked aeolian transported sediments from unit 3 (unit 2), and sandy loess deposition that capped the main body of the stringer post-deposition of unit 2 (unit 1). Outwash and locally derived sands are widely distributed throughout the area (Soil Survey Staff, 2019) and form the dominant surficial deposit along the Chippewa River and in its valley near ECC (Faulkner et al., 2016; Wisconsin DNR, 2011).

Several iron-rich concentrations (i.e., pedogenic lamellae) were observed along sedimentological boundaries within the stratified units 2 and 3. Cores 3, 4, and 6 had distinct zones of iron depletion, and all ECC cores had distinct zones of iron staining (Supplementary Tables 7-13). Numerous textural changes were also noted throughout the stringer based upon particle size data. Obear et al. (2014) studied iron-cemented

layers in golf courses around the United States and determined that iron concentrated at textural discontinuities in less than 10 years. Given the high sand content at ECC and high percolation rates in sandy deposits, couplets of iron eluviation and illuviation likely formed relatively quickly (Schaetzl and Thompson, 2015). This is comparable to the iron oxide-enriched bands observed at distinct textural changes within Canfield Creek sand stringer (Zanner, 1999). Prior geophysical investigation of ECC suggested that subtle sedimentary structures exist within the landform, possibly indicative of small ripple-like structures (Mataitis, 2020), that would result in grain-size sorting along these structures during deposition. Infiltrating water was likely getting perched at these sedimentary structure boundaries, leading to the formation of pedogenic lamellae throughout the stringer.

Radiocarbon data at ECC contain significant discrepancies from the northwest (core 1) and southeast (core 6) portions of the stringer at equivalent depths. This is not surprising given the sandy-textured nature of ECC and the notable post-depositional translocation of iron and other materials within the ECC sediments. As such, these ages can only be interpreted as limiting minimum ages given that incorporation of younger carbon likely occurred post-deposition. With that considered, radiocarbon data suggest that unit 1 deposited on top of the main stringer body (unit 2) no later than ~6300 cal yr BP. Other radiocarbon samples from this unit reveal late Holocene minimum ages. Together, these could suggest

unit 1 is a mid-late Holocene aeolian pulse(s) in this area. This is not implausible given mid and late Holocene aeolian activity has been well documented in the UMRB previously (e.g., Grigal et al., 1976; Keen and Shane, 1990; Young, 2008) and in close proximity to ECC in the Chippewa River valley (Millett, 2019). Unfortunately, OSL samples that could support or refute these minimum radiocarbon ages were not collected from unit 1 due to its shallow depth and associated concerns regarding agricultural modification. Thus, few definitive conclusions can be drawn about the significance of unit 1 at this time. In comparison, the main body of ECC, unit 2, returned OSL ages, interpreted as absolute depositional ages, ranging primarily from the Pleistocene-Holocene transition to Early Holocene (~11.3-8.9 ka; Table 3) and these will be discussed in the next section.

4.3 Geomorphic and Regional Significance of Sand Stringers in the upper Midwest, USA

GC, ECC, and CC (Zanner, 1999) sand stringers are morphologically and geographically similar. Each sand stringer exists near, but beyond the LGM glacial margins (Fig. 1), drapes underlying topography, is oriented roughly NW-SE, and has a similar elongate form. These similarities and their relative locations across the region support prior interpretations that sand stringers are ubiquitous features beyond the LGM margin in the UMRB (e.g., Hobbs, 1995; Koch and Walters, 2004; Meyer and Knaeble,

1998; Schaetzl et al., 2018; Zanner, 1999). Preliminary mapping indicates there may be several hundred of these landforms in the region (Mataitis, 2020; Zanner, 1999). These sand stringers also exist within landscapes containing numerous other poorly understood sandy aeolian landforms (e.g. parabolic dunes, sand ramps, sand sheets) (e.g., Millett, 2019; Schaetzl et al., 2018). Like these other aeolian landforms, sand stringers across the region are now stabilized, suggesting they collectively represent a former period of aeolian sediment transport and deposition.

Zanner (1999) suggested grain-size variability in the main body of his CC site, particularly in the silt fraction, was the result of ice margin fluctuations/minor readvances of the Des Moines Lobe, which was out of sync with the regional paleoclimate (Dalton et al., 2020; Heath et al., 2018; Lusardi et al., 2011). The oldest radiocarbon date, interpreted as a maximum age of ice advance in west central Iowa, indicates an advance to this area around 24 cal kyr BP (Ruhe, 1969). Ice then retreated, but the ice front likely stayed within Iowa. It later readvanced as most glacial ice was generally retreating in the UMRB (Heath et al., 2018). This later readvance of the Des Moines Lobe reached its furthest extent (near Des Moines, IA) ca. 18-17 ka (Dalton et al., 2020; Rittenour et al., 2015), or possibly as late as 16.2 cal kyr BP (Heath et al., 2018). The Des Moines Lobe retreated out of Iowa and southcentral Minnesota by ca. 14.1 ka (Lepper et al., 2013). A radiocarbon age of 14.6-13.8 cal kyr BP from wood found in proglacial lake sediments of Lake Minnesota, formed by the

retreating Des Moines Lobe, also suggests ice was far removed from the area at the time the dated stratigraphic units at CC were deposited (Jennings et al., 2012). In addition, OSL ages from another Des Moines Lobe-derived proglacial lake basin, Lake Benson, in west-central Minnesota, indicate the Des Moines Lobe had retreated entirely from southern Minnesota by 14.8 ka (Rittenour et al., 2015).

Zanner's (1999) TL ages are from a stratigraphic unit similar to the middle and upper portions of unit 1 at GC in that they appear to have experienced a coarser sediment influx as compared to the sediments beneath them. However, there are stratigraphic units delineated beneath this dated unit at CC that also contains aeolian sediments. Therefore, the true beginning of deposition of CC may be older than the TL ages Zanner reported. Assuming Zanner's TL ages (14.7±0.8, 13.7±0.9, 13.4±0.7, 13.1±0.9, 11.2±0.6 ka) from CC are accurate, except for one date (14.7 ka) they all post-date Des Moines Lobe retreat from southern Minnesota by several hundred to thousands of years. Even the oldest of these ages (14.7 ka) post-dates the Des Moines Lobe being in proximity to CC (Rittenour et al., 2015). Therefore, fine sediment fluctuations in the dated unit must have come from alternative sources – potentially areas of wasting stagnant ice and/or proglacial lake basins like Lake Minnesota after they drained. Despite this uncertainty in silt fraction fluctuations, a general coarsening upward (i.e., sandier) sedimentology was observed within the main body at CC and the TL ages come from this sandier unit.

Given the minimum ages of radiocarbon samples reported from near the base of unit 1 at GC (Fig. 4), siltier deposition of the sand stringer was occurring at least by ~25-20 cal yr BP. This time frame corresponds to regional data that suggests the Des Moines Lobe was in Iowa (Heath et al., 2018) and likely near its closest proximity to the GC site, potentially through 16.1 cal kyr BP (Dalton et al., 2020). This also corresponds to the predominant period of west-northwesterly derived loess deposition in southeastern Minnesota ca. 26-20 ka (Mason et al., 1994; Zanner, 1999). This would also have been similar for the CC site (Zanner, 1999). The lack of basal ages at CC prohibits us from determining when deposition began, but it may have started with siltier deposition in a similar timeframe to GC.

Our hypothesis is that the younger minimum radiocarbon age at GC (~9.1 ka) in the coarser, mid-to-upper, portion of unit 1, may be similar to the coarser stratigraphic unit dated by Zanner (1999) at CC. We understand there is uncertainty in these ages but given the similar general upward coarsening change at GC and CC, we hypothesize this may represent a sandier pulse of aeolian deposition beginning between ~14.7-9.1 ka. This pulse may have been incorporated into the sand stringers at a regional scale. This hypothesis is also supported by deposition of sand ramps on ridge crests and hillslopes facing northwest in southeastern Minnesota between 12.3 and 10.3 ka (Hanson et al., 2015).

ECC is a sand stringer consisting of sandy-textured aeolian sediments deposited between ca. 11.25-8.9 ka. Similarly, preliminary OSL ages from three sand stringers proximal to ECC reveal four depositional ages from sandy-textured aeolian sediments ranging from ca. 12.9 to 10.8 ka (Mataitis, 2020). ECC and the sand stringers in Mataitis (2020) were far removed from glacial ice during deposition, thus ice marginal fluctuations cannot explain deposition at these sites (Zanner, 1999). This is supported by prior work documenting glacial ice retreat from west-central Wisconsin (Clayton et al., 2001; Dalton et al., 2020; Heath et al., 2018; Syverson, 2007). ^{10}Be exposure ages from the Chippewa Lobe terminal moraine suggest retreat began after ca. 25-20 ka. Furthermore, recessional moraines to the north of the Chippewa Lobe's terminus support that ice was ~100 km further north by ca. 14.4-11.9 ka (Ullman et al., 2015). Thus, northwesterly winds (Schaetzl et al., 2018) responsible for aeolian transport and deposition were not tied to the Chippewa Lobe's position.

The eight depositional OSL ages at ECC and in Mataitis (2020) also fit the chronological period we hypothesize as a regional-scale sandy aeolian depositional pulse at CC and GC in southeastern Minnesota. In this portion of western Wisconsin, loess deposition was occurring between 18 and 13 ka (Schaetzl et al., 2014), with sediments derived from western sources (Schaetzl et al., 2021; Scull and Schaetzl, 2011). Early loess deposition may have covered much of the landscape, but currently

loess deposits are not found in this area beyond the top of isolated bedrock uplands and/or east-southeastern sides of bedrock uplands. Loess was likely deflated by saltating sands, remobilizing the loess under a west-northwest wind regime, allowing the loess to be incorporated into mobilized sands or transported to those isolated landscape positions (Schaetzl et al., 2018). The ca. 12.9 – 8.9 ka range of sand stringer ages from western Wisconsin are younger than the major loess interval, but mirror recent data emerging from a variety of sandy aeolian deposits in this same area: sand sheets ~9.2 ka; parabolic dunes ca. 10.4-10.0 ka, sand ramps ca. 10.9-10.1 ka (Millett, 2019; Schaetzl et al., 2018), sands from the base and within dunes in the central sands of Wisconsin ca. 14-10.6 ka (Rawling et al., 2008), and a ridge crest with intercalated loess and aeolian sands ca. 12.7 ka (Schaetzl et al., 2021). These data further support our hypothesis of a regional sandy aeolian pulse during the late-Pleistocene and early Holocene that impacted southeastern Minnesota and western Wisconsin far beyond the ice margin.

Unit 3 at GC remains poorly understood, but we interpret unit 3 to represent the landscape surface prior to initial deposition of GC, ca.25-20 cal kyr BP. Given observations at the other sand stringers, we can assume GC stringer draped the landscape, much like the CC and ECC stringers did. CC is underlain by glacial till that is penetrated by sand-filled, ice-wedge pseudomorphs and covered by ventifacts (Zanner, 1999). Together, these features indicate windy, periglacial conditions prior to

sand stringer deposition ca. >14.7-11.2 ka. ECC is underlain by late-Wisconsinan glaciofluvial and locally sourced sands that aggraded when the Chippewa River served as the LGM meltwater stream of the Chippewa Lobe (Faulkner et al., 2016).

It is well documented that permafrost was present and widespread throughout west-central and southwestern Wisconsin during the LGM and post-glacial period, possibly until ca. 14-12 ka (e.g., Attig and Clayton, 1986; Black, 1976, 1965, 1964; Clayton et al., 2001; Holmes and Syverson, 1997). Near ECC, recent work by Schaetzl et al. (2021) used OSL to date a type of ice-wedge pseudomorph, sand wedges, that are indicative of periglacial conditions. The ages revealed the sand that filled these wedges was deposited between ca. 19.3-14.7 ka. These ages were interpreted to represent the waning stages of the permafrost interval but are also indicative of a cold, dry, and windy environment. This is consistent with a pause in speleothem growth in southern Wisconsin (Batchelor et al., 2019) and southeastern Minnesota (Lively, 1983), interpreted to be indicative of the presence of permafrost between ca. 33-15 ka and 35-13 ka, respectively. It is likely that the surfaces underlying ECC, GC, and CC sand stringers formed in periglacial/permafrost conditions prior to the most substantial periods of sandy deposition in each stringer.

Schaetzl et al. (2021) hypothesized that OSL ages from sandy deposits in west-central Wisconsin represent the waning stages of aeolian

transport and subsequent deposition as climate warmed, vegetation became established, and soil moisture increased. Our data are in agreement with this idea. We hypothesize that as permafrost degraded throughout this region, not just in west-central Wisconsin but in southeastern Minnesota as well, sand was mobilized and transported across this region – filling ice wedge pseudomorphs. The degradation of permafrost "unlocked" stored sediment throughout the landscape and exposed it to aeolian transport – in a landscape that was dry and windy with sparse vegetation. As climate warmed and vegetation and soil moisture increased, there was a transition to aeolian deposition. The filling of ice wedge pseudomorphs may reflect the early stages of this process while cracks were open and able to store sediment. Subsequently, significant sandy aeolian deposition resulting in sand stringers, parabolic dunes, sand ramps, and sand sheets occurred later as the environment changed and surface transport slowed, sometime between ca. 14.7-8.9 ka. Importantly, this hypothesized depositional period overlaps the Younger Dryas and early Holocene and further research on sandy aeolian landforms linked to paleoenvironmental proxy records in this region may reveal broader connections between aeolian deposition and climatic transitions occurring in these timeframes. Eventually, transport ceased and these sandy aeolian forms stabilized

5. CONCLUSIONS

Based on sand stringer (McKee, 1979) morphology, stratigraphy, and chronology, it is likely that GC began forming during the LGM. This may also be true of the CC (Zanner, 1999), but geochronological data is lacking from the base of this landform. Both GC and CC generally contain coarser, sandier sediments upwards in their stratigraphic profiles. ECC formation began around the Pleistocene-Holocene transition and is entirely dominated by sandy-textured sediments. All three sand stringers formed under a predominantly northwest wind regime. Sand stringers fit an emerging regional chronology of sandy aeolian deposition ca. 13-9 ka. At and post LGM, glaciofluvial outwash sands and gravels and locally-sourced sediments made up much of the preexisting landscape over which both GC and ECC were deposited (Faulkner et al., 2016; Hobbs and Setterholm, 1998; Syverson, 2007). Peoria Loess was being transported and deposited from the west-northwest (Leigh and Knox, 1994), providing the primary sediment source for GC in addition to locally derived sands, while outwash and locally derived bedrock sands were the primary sediment sources for ECC. As permafrost began to degrade within and near the study area, outwash and locally-sourced sands on sparsely vegetated landscapes became available for aeolian transport via northwesterly winds (Schaetzl et al., 2018; Schaetzl et al., 2021). These sands are likely the main sediment source for ECC and the coarsening upwards particle size distribution (i.e., more sand) observed in the main body of GC cores below the surface soil. A generally similar coarsening

upwards particle size distribution in the main stringer body is reported at CC by Zanner (1999). This may represent a change to warmer, drier conditions (Zanner, 1999) during the interval of regional sandy aeolian deposition that waned ca. 13-9 ka - eventually quiescing due to increasing vegetation and soil moisture as climate changed (Schaetzl et al., 2021). Levels of pedogenesis at GC and ECC indicate stabilization and reduced sediment inputs during much of the Middle Holocene and Late Holocene.

Sand stringers in the UMRB, are undoubtedly a representation of paleoenvironmental change and geomorphic response to the regional deglaciation and, potentially permafrost degradation, at and post LGM. As such, landforms like aeolian sand stringers may also aid us in understanding what the future holds for some landscapes currently undergoing deglaciation and/or permafrost degradation.

DATA AVAILABILITY STATEMENT

The data that support the findings of this study are available from the corresponding author upon reasonable request.

REFERENCES

Aitken, M., Xie, J., 1990. Moisture correction for annual gamma dose. Ancient TL 8, 6–9.

Aitken, M.J., 1998. Introduction to optical dating: the dating of Quaternary sediments by the use of photon-stimulated luminescence. Clarendon Press.

Attig, J., Clayton, L., 1986. History of late Wisconsin permafrost in northern Wisconsin, in: American Quaternary Association Program and Abstracts. Presented at the American Quaternary Association Biennial Meeting, Champaign, IL, p. 115.

Batchelor, C.J., Orland, I.J., Marcott, S.A., Slaughter, R., Edwards, R.L., Zhang, P., Li, X., Cheng, H., 2019. Distinct permafrost conditions across the last two glacial periods in midlatitude North America. Geophysical Research Letters 46, 13318–13326.

Bigarella, J., 1979. Dissipation of dunes, Lagoa, Brazil, in: McKee E.D., Eds. A Study of Global Sand Seas. pp. 124–134.

Black, R.F., 1976. Periglacial features indicative of permafrost: ice and soil wedges. Quaternary Research 6, 3–26.

Black, R.F., 1965. Ice-wedge casts of Wisconsin. Transactions of the Wisconsin Academy Sciences Arts and Letters 54, 187.

Black, R.F., 1964. Periglacial phenomena of Wisconsin, north-central United States. Presented at the 6th International Congress on Quaternary (Warsaw) Report, pp. 21–27.

Breed, C.S., Grow, T., 1979. Morphology and distribution of dunes in sand seas observed by remote sensing, in: McKee E.D., Eds. A Study of Global Sand Seas. pp. 253–302.

Clark, P.U., Dyke, A.S., Shakun, J.D., Carlson, A.E., Clark, J., Wohlfarth, B., Mitrovica, J.X., Hostetler, S.W., McCabe, A.M., 2009. The Last Glacial Maximum. Science 325, 710–714.

Clayton, L., Attig, J.W., Mickelson, D.M., 2001. Effects of late Pleistocene permafrost on the landscape of Wisconsin, USA. Boreas 30, 173–188.

COHMAP Members, 1988. Climatic Changes of the Last 18,000 Years: Observations and Model Simulations. Science 241, 1043–1052. https://doi.org/10.1126/science.241.4869.1043

Dalton, A.S., Margold, M., Stokes, C.R., Tarasov, L., Dyke, A.S., Adams, R.S., Allard, S., Arends, H.E., Atkinson, N., Attig, J.W., 2020. An updated radiocarbon-based ice margin chronology for the last deglaciation of the North American Ice Sheet Complex. Quaternary Science Reviews 234, 106223.

Faulkner, D.J., Larson, P.H., Jol, H.M., Running, G.L., Loope, H.M., Goble, R.J., 2016. Autogenic incision and terrace formation resulting from abrupt late-glacial base-level fall, lower Chippewa River, Wisconsin, USA. Geomorphology 266, 75–95. https://doi.org/10.1016/j.geomorph.2016.04.016

Follmer, L.R., 1978. Soil geomorphology of northeastern Illinois; a guidebook for the joint field conference of the Soil Science Society of America and the Geological Society of America. Soil Science Society of America, United States.

Galbraith, R.F., Roberts, R.G., 2012. Statistical aspects of equivalent dose and error calculation and display in OSL dating: an overview and some recommendations. Quaternary Geochronology 11, 1–27.

Gerakis, A., Baer, B., 1999. A computer program for soil textural classification. Soil Science Society of America Journal 63, 807–808.

Grigal, D., Severson, R.C., Goltz, G., 1976. Evidence of eolian activity in north-central Minnesota 8,000 to 5,000 yr ago. Geological Society of America Bulletin 87, 1251–1254.
Guérin, G., Mercier, N., Adamiec, G., 2011. Dose-rate conversion factors: update. Ancient TL 29, 5–8.
Hanson, P., Mason, J., Jacobs, P., Young, A., 2015. Evidence for bioturbation of luminescence signals in eolian sand on upland ridgetops, southeastern Minnesota, USA. Quaternary International 362, 108–115.
Heath, S.L., Loope, H.M., Curry, B.B., Lowell, T.V., 2018. Pattern of southern Laurentide Ice Sheet margin position changes during Heinrich Stadials 2 and 1. Quaternary Science Reviews 201, 362–379.
Hobbs, H., 1995. Surficial Geology of Fillmore County, plate 3, in: Geologic Atlas of Fillmore County, Minnesota: Minnesota Geological Survey County Atlas Series C-8, Pt. A, Scale 1:100,000.
Hobbs, H., Setterholm, D.R., 1998. Surficial Geology and Thickness of Quaternary Sediments. Geologic Atlas of Goodhue County, Minnesota: Minnesota Geological Survey County Atlas Series C-12.
Holmes, M., Syverson, K., 1997. Permafrost history of Eau Claire and Chippewa Counties, Wisconsin, as indicated by ice-wedge casts. The Compass 73, 91–96.
Jennings, C.E., Lusardi, B.A., Gowan, A.S., 2012. Surficial Geology of Blue Earth County, plate 3, in: Geologic Atlas of Blue Earth County, Minnesota: Minnesota Geological Survey County Atlas Series C-26, Pt. A, Scale 1:100,000.
Keen, K.L., Shane, L.C., 1990. A continuous record of Holocene eolian activity and vegetation change at Lake Ann, east-central Minnesota. Geological Society of America Bulletin 102, 1646–1657.
Koch, J., Walters, J., 2004. LATE QUATERNARY EOLIAN SAND STRINGERS OF NORTHEAST IOWA, in: Geological Society of America Annual Meeting Abstracts with Programs, Denver, CO. Denver, CO, USA.
Krist, F., Schaetzl, R.J., 2001. Paleowind (11,000 BP) directions derived from lake spits in Northern Michigan. Geomorphology 38, 18.
Larson, P.H., Dryer, W.P., McDonald, J.M., Baker, A.C., Running, G.L., Faulkner, D.J., Jol, H.M., 2008. Geomorphology of Cliff-Top Parabolic Dunes within the Lower Chippewa River Valley, Upper Putnam Park, Eau Claire, Wisconsin, in: Abstracts with Programs. Presented at the Association of American Geographers Annual Meeting, Boston, MA.
Leigh, D., Knox, J., 1994. Loess of the Upper Mississippi Valley driftless area. Quaternary Research 42, 30–40.
Lepper, K., Buell, A.W., Fisher, T.G., Lowell, T.V., 2013. A chronology for glacial Lake Agassiz shorelines along Upham's namesake transect. Quaternary Research 80, 88–98.
Lively, R., 1983. Late Quaternary U-series speleothem growth record from southeastern Minnesota. Geology 11, 259–262.
Loope, H., 2012. Late Pleistocene eolian activity linked to permafrost degradation in the Upper Mississippi River basin, USA. Quaternary International 279, 288.
Lusardi, B.A., Jennings, C.E., Harris, K.L., 2011. Provenance of Des Moines lobe till records ice-stream catchment evolution during Laurentide deglaciation. Boreas 40, 585–597.
Mason, J.A., 2015. Up in the refrigerator: geomorphic response to periglacial environments in the Upper Mississippi River Basin, USA. Geomorphology 248, 363–381.
Mason, J.A., 1992. Loess distribution and soil landscape evolution, southeastern Minnesota.

Mason, J.A., Nater, E.A., Hobbs, H.C., 1994. Transport Direction of Wisconsinan Loess in Southeastern Minnesota. Quaternary Research 41, 41–51.
Mason, J.A., Nater, E.A., Zanner, C.W., Bell, J.C., 1999. A new model of topographic effects on the distribution of loess. Geomorphology 28, 223–236. https://doi.org/10.1016/S0169-555X(98)00112-3
Mataitis, R.J., 2020. Geomorphology and chronology of sand stringer deposition beyond the ice margin: Southeastern Minnesota and western Wisconsin, USA (Masters Thesis). Minnesota State University, Mankato, Mankato, MN.
McKee, E., 1979. A study of global sand seas. US Government Printing Office.
Meyer, G.N., Knaeble, A.R., 1998. Surficial Geology of Mower County, plate 3. Geologic atlas of Mower County, Minnesota: Minnesota Geological Survey County Atlas C-11.
Millet, J., Anzalone, C., Coonen, K., Jansen, E., Gardner, D., Larson, P., Running, G., Faulkner, D., Schirmer, R., 2018. Sandy aeolian deposition in southeastern Minnesota and western Wisconsin: A forgotten and poorly understood sandy aeolian landscape. Preliminary Results., in: American Association of Geographers Annual Meeting Abstracts. New Orleans, LA.
Millett, J., 2019. Cliff-Top Dunes in the Lower Chippewa River Valley of West-Central Wisconsin. Minnesota State University, Mankato.
Murray, A., Wintle, A., 2000. Luminescence dating of quartz using an improved single-aliquot regenerative-dose protocol. Radiation measurements 32, 57–73.
Murray, A.S., Wintle, A.G., 2000. Luminescence dating of quartz using an improved single-aliquot regenerative-dose protocol. Radiation measurements 32, 57–73.
Noller, J.S., Sowers, J.M., Lettis, W.R., 2000. Quaternary Geochronology: Methods and Applications. American Geophysical Union.
Obear, G.R., Hartemink, A.E., Soldat, D.J., 2014. Soils with iron-cemented layers on golf courses in the USA. Geoderma 232–234, 198–207. https://doi.org/10.1016/j.geoderma.2014.05.010
Olson, L.M., Larson, P.H., Huppy, J.P., Jol, H.M., Faulkner, D.J., Running, G.L., 2008. Late Quaternary Eolian Dunes and Fluvial Terraces of the Lower Chippewa River Valley, in: Abstracts with Programs. Presented at the Association of American Geographers Annual Meeting.
Prescott, J.R., Hutton, J.T., 1994. Cosmic ray contributions to dose rates for luminescence and ESR dating: large depths and long-term time variations. Radiation measurements 23, 497–500.
Rawling, J.E., Hanson, P.R., Young, A.R., Attig, J.W., 2008. Late Pleistocene dune construction in the Central Sand Plain of Wisconsin, USA. Geomorphology 100, 494–505. https://doi.org/10.1016/j.geomorph.2008.01.017
Rittenour, T.M., Cotter, J.F.P., Arends, H.E., 2015. Application of single-grain OSL dating to ice-proximal deposits, glacial Lake Benson, west-central Minnesota, USA. Quaternary Geochronology 30, 306–313. https://doi.org/10.1016/j.quageo.2015.02.025
Ruhe, R.V., 1969. Quaternary landscapes in Iowa. Iowa State Press, Ames, IA, USA.
Schaetzl, R.J., Forman, S.L., Attig, J.W., 2014. Optical ages on loess derived from outwash surfaces constrain the advance of the Laurentide Ice Sheet out of the Lake Superior Basin, USA. Quat. res. 81, 318–329. https://doi.org/10.1016/j.yqres.2013.12.003
Schaetzl, R.J., Larson, P.H., Faulkner, D.J., Running, G.L., Jol, H.M., Rittenour, T.M., 2018. Eolian sand and loess deposits indicate west-northwest paleowinds during the Late Pleistocene in western Wisconsin, USA. Quaternary Research 89, 769–785.

Schaetzl, R.J., Running IV, G., Larson, P., Rittenour, T., Yansa, C., Faulkner, D., 2021. Luminescence dating of sand wedges constrains the Late Wisconsin (MIS 2) permafrost interval in the upper Midwest, USA. Boreas.
Schaetzl, R.J., Thompson, M.L., 2015. Soils: Genesis and Geomorphology, 2nd ed. Cambridge University Press, New York, NY.
Schoeneberger, P.J., Wysocki, D.A., Benham, E.C., Soil Survey Staff, 2012. Field Book for Describing and Sampling Soils, Version 3.0. National Resources Conservation Service, National Soil Survey Center, Lincoln, NE.
Scull, P., Schaetzl, R.J., 2011. Using PCA to characterize and differentiate loess deposits in Wisconsin and Upper Michigan, USA. Geomorphology 127, 143–155.
Soil Survey Staff, 2019. Soil Survey Geographic (SSURGO) Database. Natural Resources Conservation Service, United States Department of Agriculture.
Soil Survey Staff, Natural Resources Conservation Service, U.S. Department of Agriculture, 2011. Official Soil Series Descriptions [Online] [WWW Document]. URL Available: http://soils.usda.gov/technical/classification/osd/index.html (accessed 3.22.22).
Stanley, K.E., Schaetzl, R.J., 2011. Characteristics and paleoenvironmental significance of a thin, dual-sourced loess sheet, north-central Wisconsin. Aeolian Research 2, 241–251. https://doi.org/10.1016/j.aeolia.2011.01.001
Stuiver, M., 1980. Workshop on 14C data reporting. Radiocarbon 22, 964–966.
Stuiver, M., Polach, H.A., 1977. Discussion reporting of 14C data. Radiocarbon 19, 355–363.
Stuiver, M., Reimer, P.J., Reimer, R.W., 2021. CALIB 8.2 [WWW program]. URL http://calib.org (accessed 1.15.21).
Syverson, K.M., 2007. Pleistocene Geology of Chippewa County, Wisconsin. Wisconsin Geological and Natural History Survey.
Thorp, J., Smith, H.T.U., 1952. Pleistocene eolian deposits of the United States, Alaska and parts of Canada. National Research Council Committee for the Study of Eolian Deposits.
Ullman, D.J., Carlson, A.E., LeGrande, A.N., Anslow, F.S., Moore, A.K., Caffee, M., Syverson, K.M., Licciardi, J.M., 2015. Southern Laurentide ice-sheet retreat synchronous with rising boreal summer insolation. Geology 43, 23–26.
Vader, M.J., Zeman, B.K., Schaetzl, R.J., Anderson, K.L., Walquist, R.W., Freiberger, K.M., Emmendorfer, J.A., Wang, H., 2012. Proxy Evidence for Easterly Winds in Glacial Lake Algonquin, from the Black River Delta in Northern Lower Michigan. Physical Geography 33, 252–268. https://doi.org/10.2747/0272-3646.33.3.252
Wisconsin DNR, 2011. Surficial Deposits. Ecological Landscapes of Wisconsin Handbook.
Young, A.R., 2008. Alluvial and Eolian Depositional History of the Barrens Fan Northwestern Wisconsin (Masters Thesis). University of Nebraska Lincoln.
Zanner, C.W., 1999. Late-Quaternary landscape evolution in southeastern Minnesota: Loess, eolian sand, and the periglacial environment. University of Minnesota.

Table 1. GC and ECC sand stringer soil-sediment core information.

Core	Elevation (m)	Sand Stringer Geomorphic Position	Core Depth (cm)
GC sand stringer (44.460820° N, 92.703660° W)			
1	313.55	South-east facing slope	282
2	312.16	South-east facing slope	241
3	313.25	Northwest-facing slope/swale	313
4	317.79	Crest	199
5	316.43	Secondary peak to north	172
6	310.06	Valley floor to south	145
ECC sand stringer (44.798570° N, 91.595660° W)			
1	271.70	Crest	186
2	271.60	Shoulder (north)	197
3	272.86	Shoulder (south)	274
4	273.00	Crest	177
5	272.90	Shoulder (north)	198
6	273.83	Crest	289
7	271.50	Valley floor to south	177

Table 2. Radiocarbon ages for GC and ECC sand stringers. Calendar ages calibrated using the online CALIB 8.2 Radiocarbon Calibration Program; ages rounded to the nearest decade.

Core Name	Depth (cm)	Soil Horizon	Lab Number	$\delta^{13}C$ (‰)	^{14}C age (yr BP ± 1σ)	Calendar age (yr BP ± 2σ)
ECC 1	61	BC	OS-159317	-21.30	1,410 ± 20	1,310 ± 10
ECC 6	91	2C stratified	OS-157918	-18.95	2,050 ± 20	1,990 ± 60
ECC 1	94	2C stratified	OS-157917	-19.84	5,470 ± 30	6,290 ± 20
ECC 1	128	2C stratified	OS-159383	-22.39	7,210 ± 35	7,990 ± 50
GC 3	118	C2	OS-159319	-23.13	8,190 ± 30	9,090 ± 60
GC 6	122	3C	OS-158458	-19.92	17,900 ± 210	21,660 ± 590
GC 2	188	C2	OS-159318	-23.87	18,500 ± 110	22,470 ± 290
GC 3	216	2C	OS-158459	-24.31	21,100 ± 310	25,290 ± 670
GC 2	235	3C	OS-157919	-19.48	16,650 ± 160	20,130 ± 350

Table 3. Optically stimulated luminescence age information for ECC sand stringer.

Core	Lab Sample Number	Depth (cm)	Num. of Aliqouts[1]	Dose rate (Gy/kyr)	Equivalent dose[2] ± 2σ (Gy)	OSL age ± 2σ (ka)
ECC 6	USU-3024	145	19 (32)	1.60 ± 0.06	14.17 ± 1.94	8.86 ± 1.40
ECC 1	USU-3025	153	23 (31)	1.28 ± 0.05	14.27 ± 1.75	11.17 ± 1.64
ECC 1	USU-3026	242	20 (27)	1.78 ± 0.07	18.01 ± 1.81	10.14 ± 1.30
ECC 1	USU-3027	275	17 (27)	1.40 ± 0.05	15.71 ± 2.02	11.25 ± 1.71

[1]Age analysis using the single-aliquot regenerative-dose procedure of Murray and Wintle (2000) on 2mm small-aliquots of quart sand (150-250 μm). Number of aliquots used in age calculation and number of aliquots analyzed in parentheses.

[2]Equivalent dose (D_E) calculated using Central Age Model (CAM) and Galbraith and Roberts (2012).

Table 4. Optically stimulated luminescence dose rate data for ECC sand stringer.

Lab Sample Number	In-situ H_2O (%)[1]	K (%)[2]	Rb (ppm)[2]	Th (ppm)[2]	U (ppm)[2]	Cosmic (Gy/ka)
USU-3024	8.9	1.33±0.03	33.8±1.4	1.7±0.2	0.5±0.1	0.18±0.02
USU-3025	8.9	0.91±0.02	24.1±1.0	1.9±0.2	0.6±0.1	0.18±0.02
USU-3026	9.7	1.55±0.04	36.5±1.5	1.7±0.2	0.5±0.1	0.16±0.02
USU-3027	9.1	1.13±0.03	29.6±1.2	1.8±0.2	0.5±0.1	0.16±0.02

[1]Assumed 8.0±2.4% for all samples as moisture content over burial history.
[2]Radioelemental concentrations determined by ALS Chemex using ICP-MS and ICP-AES techniques; dose rate is derived from concentrations by conversion factors from Guérin et al. (2011).

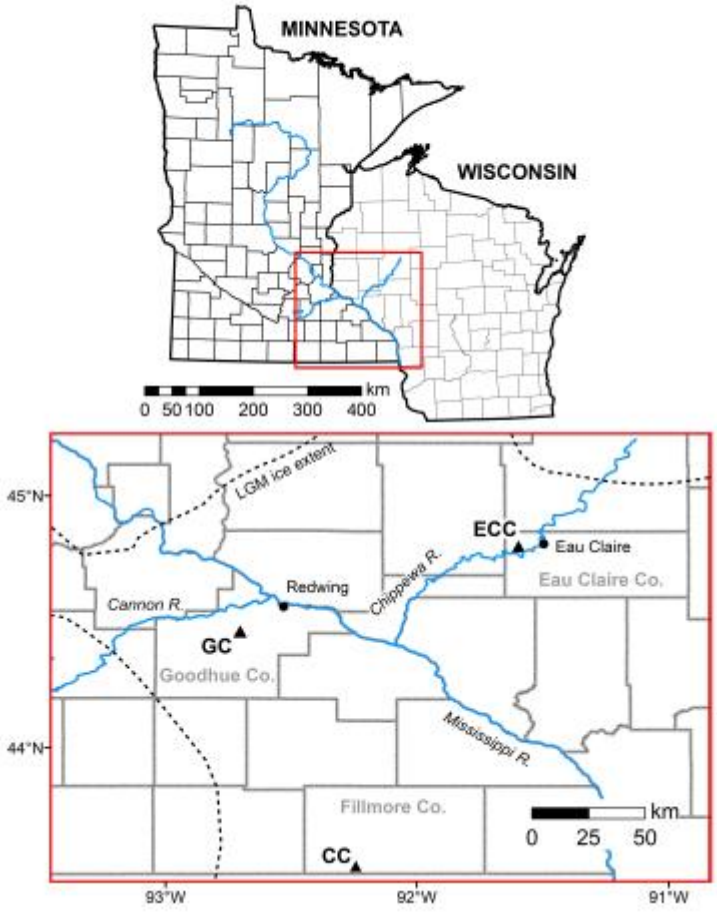

Figure 1. Location of GC, ECC, and CC (Zanner, 1999) sand stringers. Last Glacial Maximum (LGM) glacial ice extent at 21.7 cal kyr BP from Dalton et al. (2020).

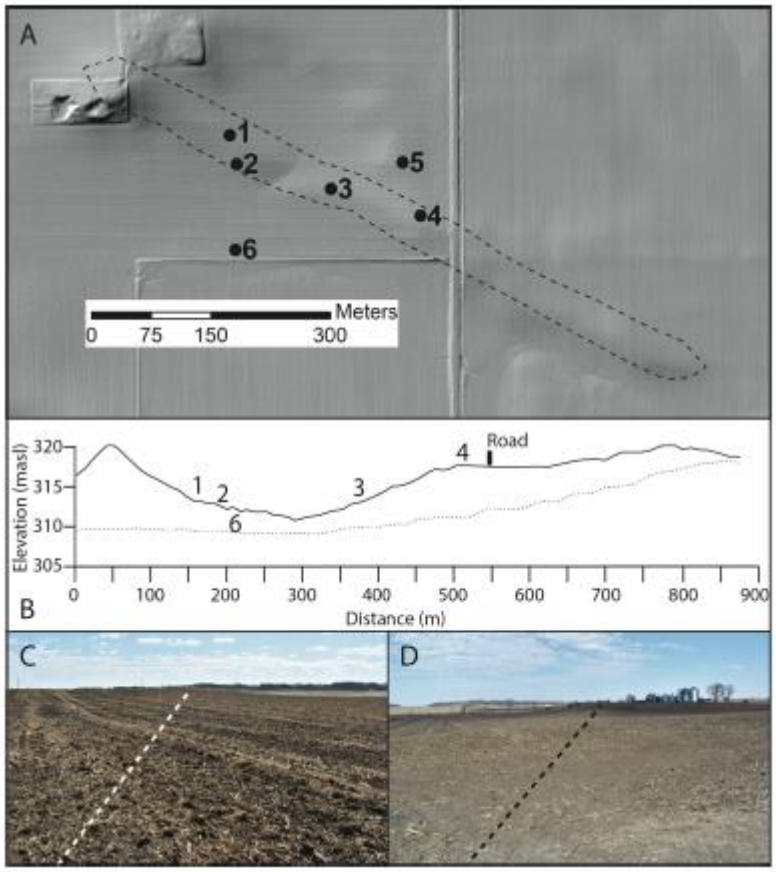

Figure 2. GC sand stringer (a) LiDAR hillshade digital elevation model with core locations (circles) and stringer boundary (dashed line), (b) topographic profile (~10X vertical exaggeration) with core locations (numbers) for the stringer long axis (solid line) and valley floor immediately south of stringer (dashed line) showing a pronounced swale within the sand stringer and elevation of the valley floor increasing to the southeast, (c) ground imagery looking southeast down the crest from west of core 3 towards core 4 (dashed line follows crest), and (d) ground imagery looking northwest down the crest from the road immediately east of core 4 (dashed line follows crest).

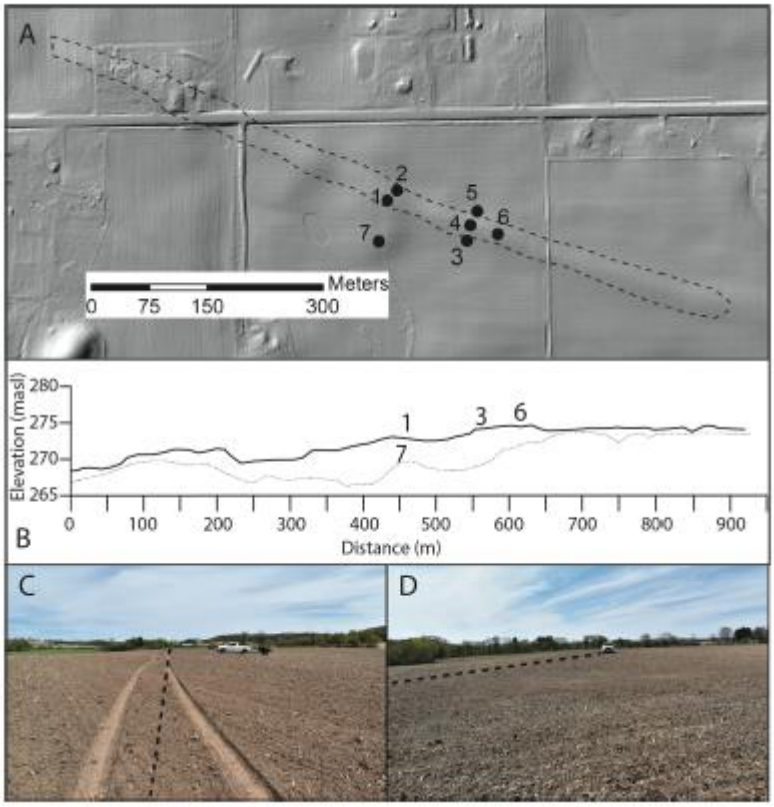

Figure 3. ECC sand stringer (a) LiDAR hillshade digital elevation model with core locations (circles) and stringer boundary (dashed line), (b) topographic profile (~10X vertical exaggeration) with core locations (numbers) for the stringer long axis (solid line) and valley floor immediately south of the stringer (dashed line) showing gently undulating topography with elevation increasing to the southeast, (c) ground imagery looking southeast down the crest from immediately west of core 4 (truck is positioned at core 3) (dashed line follows crest), and (d) ground image looking west from northeast of core 6 (truck is positioned at core 5) (dashed line follows crest).

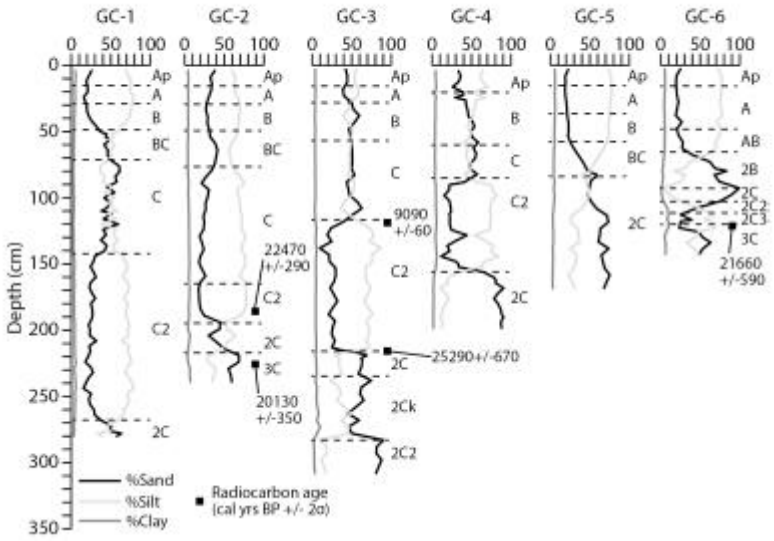

Figure 4. Percent sand, silt, and clay and soil horizonation for all GC sand stringer cores with radiocarbon (^{14}C) ages calibrated to calendar years. For soil horizons, prefix 2 indicates unit 2 and prefix 3 indicates unit 3.

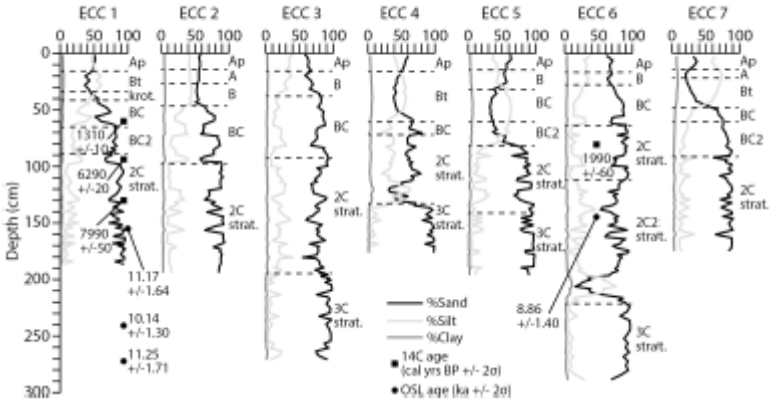

Figure 5. Percent sand, silt, and clay and soil horizonation for all ECC sand stringer cores with radiocarbon (^{14}C) ages calibrated to calendar years and optically stimulated luminescence (OSL) ages. Stratified units (i.e., 2C strat. and 3C strat.) consist of 1-10-cm-thick intercalated layers of sand, loamy sand, and sandy loam. For soil horizons, prefix 2 indicates unit 2 and prefix 3 indicates unit 3.

GRAPHICAL ABSTRACT

MORPHOLOGY AND STRATIGRAPHY OF AEOLIAN SAND STRINGERS IN SOUTHEAST MINNESOTA AND WESTERN WISCONSIN, USA

*Kenzie L. Shandonay 1 , Mark W. Bowen 2 , Phillip H. Larson 2 , Garry L. Running 3 , Tammy Rittenour 4 , Richard Mataitis 2
(1) School of Geographical Sciences and Urban Planning, Arizona State University, Tempe, AZ, 85282, (2) Department of Geography, Earth Science Programs, and EARTH Systems Laboratory, Minnesota State University, Mankato, Mankato, MN 56001, (3) Department of Geography and Anthropology, University of Wisconsin-Eau Claire, Eau Claire, WI 54701, (4) Department of Geosciences, Luminescence Laboratory, Utah State University, Logan, UT 84322

Sand stringers are common across the upper Mississippi River basin, USA. Sand stringers were deposited beyond the LGM margin and may be linked to a hypothesized sandy aeolian pulse contemporaneous with permafrost degradation. GC contains an upward coarsening in the main body of the stringer and ECC is predominantly sandy throughout. OSL ages (11.25-8.9 ka) from ECC are similar to regional sandy aeolian depositional ages in prior research. ^{14}C ages from both locations suggest deposition at or post LGM.